Research Square

Preprints are preliminary reports that have not undergone peer review.
They should not be considered conclusive, used to inform clinical practice,
or referenced by the media as validated information.

Machine learning-guided discovery of ionic polymer electrolytes for lithium metal batteries

Kai Li
Fudan University
Jifeng Wang
Fudan University
Yuanyuan Song
Fudan University
Ying Wang (wying@fudan.edu.cn)
Fudan University https://orcid.org/0000-0002-7459-1152

Article

Keywords:

Posted Date: November 9th, 2022

DOI: https://doi.org/10.21203/rs.3.rs-2220925/v1

License: This work is licensed under a Creative Commons Attribution 4.0 International License.
Read Full License

Version of Record: A version of this preprint was published at Nature Communications on May 15th, 2023. See the published version at https://doi.org/10.1038/s41467-023-38493-7.

Abstract

Development of ionic polymer electrolytes (IPEs) without flammable organics is a critical strategy to enable safe and high-energy lithium metal batteries (LMBs). As critical components in IPEs, ionic liquids (ILs) with high ionic conductivity and wide electrochemical window are promising candidates to enable LMBs. Here, we describe a fast and robust machine learning workflow embedded with quantum chemistry calculation and graph convolutional neural network to discover promising ILs for IPEs. By selecting subsets of the recommended ILs, combining with a rigid-rod polyelectrolyte and a predetermined lithium salt, we develop a class of large area and mechanically strong IPE membranes with thickness ~ 50 μm. The symmetric cells exhibit stable cycling performance at 1 mA cm^{-1} (0.5 mAh cm^{-2}) up to 800 h at room temperature (RT) and excellent reversibility at 6 mA cm^{-2} (3 mAh cm^{-2}) at 80 °C. With $LiFePO_4$ loading ~ 10.3 mg cm^{-2}, the full cells deliver outstanding capacity retention for > 350 cycles (> 96% with 0.5 C at RT; > 80% with 2 C at 50 °C), fast charge/discharge capability (146 mAh g^{-1} with 5 C at 80 °C) and ultrahigh coulombic efficiency (> 99.92%). This performance is rarely reported by any single-layer polymer electrolytes without any organic plasticizers/oligomers for LMBs.

Full Text

Ionic polymer electrolytes (IPEs) containing the non-flammable ions embedded with the mechanically supporting polymers with predetermined ionic pathway have received considerable attention toward reviving clean energy storage and conversion devices, such as batteries,[1-6] fuel cells,[7] supercapacitors,[8] mechanical actuators[9] and reverse osmosis membranes.[10] As promising candidates for safe and environmentally friendly electrolyte materials, ionic liquids (ILs) are room temperature (RT) molten salts with low vapor pressure, high thermal stability, wide electrochemical window and high ionic conductivity.[1,5,11] In recent years, liquid crystalline polymers have shown the capability to effectively reduce the interfacial resistance, meanwhile raising unique ion conduction mechanisms in lithium metal batteries (LMBs).[1,12] Li metal anode coupled with high-energy-density cathodes, for example Li-air and Li-sulfur batteries, usually require highly conductive, thermal-stable and electrochemical-stable electrolytes to suppress inhomogeneous Li dendrites, overcome the side reactions and break the tradeoff between conductivity and modulus in the composite electrolytes.[13,14] To alleviate these issues synergistically, IPEs have shown the capability to block dendrites through the robust polymer matrix, meanwhile guarantee the extreme safety by avoiding organic plasticizer in LMBs.[13,15-17]

As critical components in IPEs, it is desirable to develop a method to screen suitable ILs from a large population of ion pairs to develop successful IPEs for LMBs. ML has been widely discussed to predict properties and learn the rules underlying datasets, thus efficiently simplifying the material-discovery process.[18-23] Here, we describe a machine learning (ML) workflow embedded with the quantum chemistry calculation and graph convolutional neural network (GCN) to discover potential ILs with high ionic conductivity and sufficient electrochemical window. Driven by the structure-property relationships, previous researchers have developed diverse statistical methods and regression models to predict

physical properties, for example, melting point[24], viscosity[25] and ionic conductivity[26] based on the structure descriptors of the ILs.[27] However, the reported high accuracy usually originates from the overfitting of the dataset.[28,29] Among the training datasets, the sample size of unique ILs is extremely limited.[27,28] The investigated datasets usually contain the datapoints of the same ILs at varying temperatures, these replicated datapoints will increase the appeal accuracy of the reported models artificially. [25,30] Thus, it is still challenging to predict the accurate properties of new ILs without enough labeled datapoints and preparation of featured factors for the explanatory variables. However, to overcome the data scarcity issue, we can specifically focus on the design of statistical regression and classification workflow to discover new applicable ILs instead of predicting the absolute physical properties of the IL pairs, thus will relief the issue of data scarcity in practical application of ML in material science. In addition, this work also demonstrates the efficiency to use GCN for the graph classification task based on the graph-to-property relationship of ILs.

Based on the screening results from ML, we experimentally investigate some of the filtered ILs combined with a liquid crystalline polyelectrolyte Poly 2,2'-disulfonyl-4,4'-benzidine terephthalamide (PBDT) and a predetermined Li salt to develop a series of IPEs. As reported previously, Li metal anode shows highly reversible cycling-performance with a stable solid-electrolyte interphase (SEI) formed by electrochemically reduction of the bis(fluorosulfonyl)imide (FSI^-) anion.[31,32] Thus, we employ LiFSI dissolved in ILs as an ion exchange medium to load Li ions in the IPEs. By incorporating these IPEs into batteries with Li metal as an anode, we can experimentally confirm the properties of these developed IPEs, including thermal stability, ionic conductivity, Li^+ transference number, electrochemical window and Li dendrite suppression.

Machine Learning-guided Screening Of Ionic Liquids

This machine learning workflow requires two main steps: (1) Unsupervised learning, followed by (2) Supervised learning to target promising ILs. As shown in Fig. 1, we obtain 76 cations and 31 anions from the web scrapping of IoLiTech website. The permutation of cations and anions forms an ionic liquid pool containing 2356 unique ILs, but only less than 13% of the ILs showing measured properties, for example melting point, viscosity, conductivity and electrochemical window. Three open-source platforms, including RDKit, Psi4 and Pytorch Geometrics (PyG), have been employed to generate the molecular descriptors of the raw dataset. RDKit is a powerful tool to calculate the molecular structure and three dimensional (3D) descriptors of the molecules.[33] Psi4 is an open-source ab initio electronic structure program for high-throughput quantum chemistry.[34] We employ the self-consistence field (SCF) method along with the basis set of 6-311 + G** to optimize the geometric structure and then calcualte the energy, the highest occupied molecular orbital energy (E_{HOMO}), the lowest unoccupied molecular orbital energy (E_{LUMO}) and the molecular dipole moment for the cations and anions seperately. In this work, we combine 60 molecular structure descriptors from RDKit and 14 calculated variables from Psi4 for cations, anions in the final dataset. PyG is a library based on Pytorch to build and train Graph Neural Networks (GNN) for a wide range of prediction tasks. For the unsupervised learning, we employ boxplots, pair plots and

hierarchical clustering to summarize the basic rules underlying the dataset. In terms of the supervised learning, we employ both statistical regression and classification to promote the screening efficiency. Among the 2356 ILs, we initially use the classification method to predict the state (solid/liquid) of the ion pairs at RT. Then we employ both statistical regression and classification to evaluate the conductivity of the obtained 1240 ILs (liquid at RT). As we expected, it is particularly challenging to obtain the absolute conductivity of the ILs with high accuracy through regression, especially for the ions with small samples in the training model. To improve the screening efficiency, we utilize a complementary classification method, which will classify the ILs into two categories, based on predetermined and tunable threshold of conductivity, thus will alleviate the low accuracy arises from the limited datapoints. The ensemble learning is based on the combination of algorithms including support vector machine (SVM), random forest (RF), XGBoosting (XGB) and GCN. The last screening step is determined by the computed electrochemical window value (ECW) according to Eq. 1–3 through Psi4. The ECW of an IL is determined by both cations and anions. The cathodic limit (V_{CL}) is the maximum value of the cathodic potential determined by the E_{LUMO} for cations and anions. Similarly, the anodic limit (V_{AL}) is the minimum value of the anodic potential determined by the E_{HOMO} for cations and anions.[35] According to this machine learning workflow shown in Fig. 1, we finally obtain 40 ILs in the recommendation list. We will expand the discussion of the unsupervised learning and the supervised learning in the following sections.

$$V_{CL} = \max\left(-\frac{E_{LUMO}[+]}{e}, -\frac{E_{LUMO}[-]}{e}\right) \text{ Eq. (1)}$$

$$V_{AL} = \min\left(-\frac{E_{HOMO}[+]}{e}, -\frac{E_{HOMO}[-]}{e}\right) \text{ Equation (2)}$$

$$\mathrm{ECW} = V_{AL} - V_{CL} \text{ Eq. (3)}$$

Unsupervised Learning

To investigate the features and the underlying correlations in the dataset, we employ the unsupervised learning as a feature detector. Figure 2a,b display the boxplots of the ILs with known σ in the dataset, which are classified by the cation and anion types correspondingly. In terms of the cations, the average σ follows the order of ammonium > sulfonium > pyrrolidinium > imidazolium > pyridinium > piperidinium > phosphonium. Accordingly, the rule for the anions is nitrate > thiocyanate > DCA > BF_4 > triflate > sulfate > imide > sulfonate > acetate > halogen > phosph. Figure 2c,d display the rankings for the measured ECW of the ILs correspondingly. We observe that the ECW boxplots showing large variations, but the ammonium-based cations and imide-based anions commonly displaying promissing ECWs. In order to understand the corelations between different features, as shown in Fig. 2e, we observe that the σ is highly corelated with the viscosity of ILs, which can be elucidated by Nernst-Einstein equation and Stokes-Einstein equation included in Supplementary Note 1.[36] However, as shown in Fig. 2f, there is no strong corelation between σ and ECW. Thus, we can conclude that σ and ECW of ILs are two independent features. As we familar, both σ and ECW are essential properties for electrolytes applied for LMBs. Zhang[30] has employed

hierachical clustering to predict fast inorganic Li ion conductors. Here, we also employ this algorithm to detect the clusters of ILs with high conductivity and wide ECW. The key features used for the hierachical clustering include the computed ECW and the top 10 factors obtained from the XGBoosting model for conductivity classification (Supplementary Note 2). The clustering criterior is a combination of the σ and the ECW of the ILs. The final results are shown in Fig. 2g. Additionally, in order to validate the effectiveness of the clustering, we also plot the finally screened ILs based on the supervised learning in Fig. 2h, we can clearly observe that the results based on the two learning protocols are highly overlaped, which indicates the high efficiency of the unsupervised learning as compared to the supervised learning introduced in the following section.

Supervised Learning

Building on the unsupervised learning, we initially propose a complementary supervised learning to filter ILs with liquid phase at RT based on the ensemble learning of SVM, RF, XGB and GCN. The classification results are shown in the Supplementary Note 3. Figure 3a indicates the corelation between the radius of gyration for anion and the heavy atom molecular weight for the classified solid and liquid groups, we observe that the ILs with high sphericity tend to be in solid state, whereras those with high asymmetry of anions will usually turn to be liquid state. We also include the top 10 importance features of XGB model in Fig. 3b. As we expected, the phase of ILs are highly dependent on the gyometic strucutres of anions. To further validate the predicted results, we employ quantum chemistry calculation to calculate the interaction energy between cations and anions. We randomly select 20 ILs from the predicted solid and liquid groups, seperately. The interaction energies of the selected ion pairs are calculated based on Eq. 4. As shown in Fig. 3c, the interaction energies for the solid ILs are generally lower compared to the liquid ILs. The detailed calculation results are included in Supplementary Table 1. As we know, the interaction energy of the cation and anion is the energy required to combine cation and anion. The lower of the interaction energies means easier for the cations and anions to stay in tightly associated pairs. In addition, we also employ GCN model to investigate this classification. The workflow of the GCN model is shown in Fig. 3d. The details about the GCN model used in this work are also included in the Supplementary Note 4. The efficiencies of employed models are included in Table 1. We observe that the GCN model offers similar performance only based on the chemcial geometric descriptors without any additional calculation results, which shows high promise for this algotihrm for future materials genome projects. Additionally, we also apply the other three models to predict the absolute σ of the liquid (1084) ILs pairs at RT. The boxplots shown in Fig. 3e further indicate the consistency between the regression and the classification results. The median value of the predicted conductivity for cluster with $\sigma < 5$ is 1.9 mS cm^{-1}. Meanwhile, the median value for cluster with $\sigma \geq 5$ is 8.9 mS cm^{-1}. Finally, we propose 40 ILs with $\sigma \geq 5$ mS cm^{-1} along with an satisfactory ECW > 3.5 V in the final recommendation list for development of IPE in LMBs. The full list is included in Supplementary Table 2. The bubble plots shown in Fig. 3f, g indicate the distribution of the filtered ILs based on the cation and anion types, correspondingly. In terms of the cations, we observe that the imidazolium cations display the highest average ionic conductivity. In terms of the anions, BF_4, sulfate and triflate show both promising ECW and σ. Base on this prliminary

rules, we select four widely discussed ILs from the bubbles and conduct experimetanl validation in the following section.

$$\mathrm{E}_{interactionenergy} = \mathrm{E}_{[+][-]} - \mathrm{E}_{[+]} - \mathrm{E}_{[-]} \quad \textbf{Eq. (4)}$$

Table 1
The performance of the classification tasks based on different algorithms.

Algorithm	R^2 (Solid or Liquid)	R^2(σ ≥ 5 or σ < 5)
Support Vector Machine (SVM)	0.80	0.82
Random Forest (RF)	0.85	0.81
XGBoosting (XGB)	0.86	0.81
Graph Convolutional Neural Network (GCN)	0.83	NA

*The R^2 for SVM, RF and XGB algorithms are the avergae of the 5-fold cross-validation accuracy results.

Electrochemical Performance Of Ipes Based On The Filtered Il

To verify the efficiency of this screening process, we develop a series of IPEs based on 4 hydrophilic ILs on the final recommendation list and validate the cycling behavior and electrochemical performance of the developed IPEs coupled with the Li metal anodes. The selected ILs include 1-ethyl-3-methylimidazolium triflate (C_2mimTFO), 1-ethyl-3-methylimidazolium tetrafluoroborate (C_2mimBF_4), 1-ethyl-3-methylimidazolium ethyl sulfate (C_2mimEthylSulfate) and diethylmethylammonium triflate (DemaTFO). All these ILs are hydrophilic and showing high ionic conductivity at RT, we can use solvent-casting method to prepare ultrathin (~ 50 μm) polymer electrolytes as reported previously.[1,6,37] The fabricated films are transparent and mechanically strong with 5/10wt% of PBDT. After ion exchange with the ionic liquid electrolyte (ILE) with LiFSI dissolved in N-propyl-N-methylpyrrolidinium bis(fluorosulfonyl)imide (C_3mpyrFSI), we obtain large area and flexible IPE membranes. The solid-state membrane electrolytes with diameter of 9 mm shown as insets in Fig. 4a-c are assembled in LMBs. Initially, we perform cyclic voltammetry (CV) on Li|IPEs|SUS to evaluate the Li plating (negative scan) and stripping (positive scan) behavior of the selected ILs combined with PBDT. We observe that upon scanning in the negative direction, this electrolyte displays excellent cathodic stability for Li-metal cycling. The achieved high current density offers promise for these IPEs as conductive electrolytes in LMBs. Among the four ILs, only DemaTFO displays no Li deposition in the cathodic deposition, which indicates that the ion exchange protocol fails to incorporate Li ions in DemaTFO based IPEs. Thus, we conclude that the ion association behavior and varying interaction energies are essential factors to determine the final chemical composition in the IPEs. In the following discussion, we will only focus on the other three IPEs. For the positive direction, as shown in the enlarged curves in the insets, we observe that C_2mimTFO based IPEs show the highest anodic stability up to 5 V vs Li|Li^+, which confirms the high

electrochemical stability of IPEs based on C_2mimTFO. However, both BF_4^- and Ethyl Sulfate display fluctuate current starting from 4V for BF_4 and 3.5V for Ethyl Sulfate, which are lower compared to the computed ECWs. As reported previously, the calculated anodic limits for BF_4^- are usually overestimated using the vacuum calculation model compared to the experimental results.[35] The reasons for the inconsistency originate from many factors, for example the assumption of the calculation model and the complicated ion association in the real system. For comparison, we include the CV results for the three neat ILs in Supplementary Note 5. Surprisingly, the cathodic limits for the neat ILs are much lower compared to the IPEs. We propose that the high Li^+ concentration and PBDT in the IPEs can improve the cathodic stability of the composite electrolytes, which is analogy to the “water in salt” electrolytes proposed by Suo et al.[38] The solvation of the Li^+, cations and anions will change dramatically with the adjustment of the relative ion concentrations. We have demonstrated that the rigid-rod polyelectrolyte PBDT backbone will selectively absorb cations and anions during the ion exchange process, which will promote the Li transference number (t_{Li}^+) of the system. Here, we estimate the t_{Li}^+ based on the steady-state current of the Li symmetric cell assembled with IPEs as electrolyte and separator in Fig. 4d. The insets show the corresponding impedance spectra of the cells before and after the polarization. The t_{Li}^+ of Bruce-Vincent analysis is defined in Supplementary Note 6.[39] The determined t_{Li}^+ in these IPEs (0.4–0.5) are much higher compared to the pure ILE with LiFSI|C_3mpyrFSI (t_{Li}^+ = 0.18)[40]. Among these three IPEs, C_2mimTFO based IPEs show higher t_{Li}^+= 0.5 compared to C_2mimBF_4 (0.4) and Dema Ethyl Sulfate (0.4) for the varying interaction between PBDT chains and the anions in ILs. We are conducting in depth quantum chemistry calculations to measure the interaction energies between anions and PBDT polymer chains, thus will offer more clear idea about the determining factors in the ion exchange process. Figure 4e shows ionic conductivities of the IPEs as a function of temperature. The exceedingly high σ at RT (> 1 mS cm^{-1}) originates from the fibrillar and nanocrystalline conducting phase formed in the composite structure of IL and liquid-crystalline polymers reported previously.[1,6] Meanwhile, all samples show stable Li stripping and plating at varying current grades in the Li||Li cell cycling process. As shown in Fig. 4f, C_2mimTFO and C_2mim Ethyl Sulfate display stable cycling at high current density (J) at 6 mA cm^{-2} at 80°C, which is promising, since most organic cells reported cannot sustain any stable performance at this high temperature without any safety concerns.

In this section, we mainly extend the investigation of IPEs based on C_2mimTFO at varying temperature and cell configurations. In Fig. 5a, we initially test the symmetric cell performance at varying J at RT. The critical J is 2.0 mA cm^{-2} at RT. As shown in Fig. 5b, the cells can maintain at least 800 hours at 1 mA cm^{-2} at RT, which is rarely seen by other single-layer polymer electrolytes without any supporting separators or organic plastiziers.[41] In addition, we prepare the Li|IPEs|Cu cell to investigate the plating and striping of Li at the Cu anode based on these IPEs. Figure 5b shows the voltage-cycle profile for the cells at RT. The secondary axis shows the corresponding columbic efficiency (CE) values, the average value of which is > 98%. The reported average CE for Li||Cu cell using regular organic electrolytes is ~ 90%, which indicates the highly reversible Li deposition on Cu surface of these IPEs.[42–44] The SEM

images of the deposited Li on current collector is included in the Supplementary Note 7. We observe no Li dendrites formed using these IPEs coupled with Li metal anodes.

For practical application, we also report the full cell performance based on the commercial $LiFePO_4$ cathode with high loading (10.3 mg cm^{-2}). Figure 6a shows the long-term cycling of the full cell at RT at 0.5 C rate, the cell shows 96% capacity retention at 350 cycle. The voltage capacity files for the selected main cycles are shown in Fig. 6b. The major population of the CE is between 100.1% – 100.2%, which is slightly higher than the theoretical maximum value (100%) because of the thermal fluctuation at the ambient temperature. Thus indicates the high reversibility of the Li metal cells based on this IPEs at RT. Figure 6c shows the long-term cycling of the full cell at 50°C at 2 C rate, the cell shows not only high average CE (> 99.9), but also 80% capacity retention at 350th cycle, which is promising to satisfy the fast charge/discharge requirements for widely used portable devices. The voltage capacity files for the selected main cycles are shown in Fig. 6d. At last, we also investigate the fast charge/discharge capability and thermal stability of this IPEs at 80°C, which is a dangerous temperature for regular organic cells. Figure 6e shows the cycling performance of the IPE at increasing C rate from 0.5 C (0.53mA/cm2) to 5 C (5.3 mA cm^{-2})) at 80°C. Here, we observe that the cell can cycle without short circuit at super high *J* up to 5C (8.3 mA cm^{-2}), which show promise for this IPEs as next-generation solid-state electrolytes for fast charge LMBs at mid-high temperatures. The corresponding voltage capacity curves for the selected cycles are shown in Fig. 6f.

In summary, we have described a machine learning-guided screening protocol to filter promising ILs with high ionic conductivity and wide electrochemical window for preparation of IPEs in LMBs. In addition, we further confirm the rigid-rod liquid crystalline polyelectrolyte PBDT as an essential polymer matrix to develop a series of solid-state polymer electrolytes with extremely high CE and excellent fast charge and discharge performance at high temperature. This platform shows immense potential to serve as an efficient method to quickly focus on the essential ionic liquids for specific applications. More importantly, this work provides novel insights into strategies to overcome the data scarcity issues and realize the efficient utilization of ML in material design and optimization. Through investigation of the golden rules, we could fabricate IPEs with tunable variations in mechanical, structural and transport properties for a large array of applications in versatile functional devices, including capacitors, mechanical actuators, water reverse osmosis membranes and so on.

Methods

Machine Learning

Python programming language was used to conduct the machine learning workflow. For the unsupervised learning, Dendrogram function from the SciPy package was used to perform the agglomerative hierarchical clustering. For the supervised learning, three main algorithms, including support vector machine, random forest and XGBoosting from the Scikit-learn package were used for the regression and classification. Graph convolutional neural network (GCN) has been employed to conduct

the classification in the supervised learning according to the RDkit and PyTorch Geometic (PyG) library. The machine learning workflow mainly consists of 8 sections, the code for each section were packaged in a Class object and the description of the codes are available at the GitHub website.

Quantum chemistry calculation

All quantum chemistry calculation were performed using Psi4 based on self-consistence field method with basis set of 6-311 + g**. The Psikit module, which is an ensemble of RDkit and Psi4, has been used to connect and perform the calculation of the energy, the HOMO, the LUMO, the total dipole moment and the individual dipole moments along the three main directions for the cations and anions in the IL permutation table.

Materials

Poly 2,2'-disulfonyl-4,4'-benzidine terephthalamide (PBDT) was synthesized by interfacial condensation polymerization as described previously.[45,46] 1-ethyl-3-methylimidazolium triflate, 1-ethyl-3-methylimidazolium tetrafluoroborate, 1-ethyl-3-methylimidazolium ethyl sulfate and diethylmethylammonium triflate were purchased from IoliTech. N-propyl-N-methylpyrrolidinium bis(fluorosulfonyl)imide (C_3mpyrFSI, purity > 99.9%) and Lithium bis(fluorosulfonyl)imide (LiFSI, purity > 99.5%) were purchased from Solvionic. Lithium metal (Li-metal) foil with thickness of 180 μm was sourced from Hongwei Lithium Co. Ltd. (purity > 99.9%). The $LiFePO_4$ cathode with area loading of 10.3 mg cm^{-2} and Cu foil were sourced from Canrd.

Preparation of the ionic polymer electrolytes (IPEs)

0.45 g ILs and 0.05 g PBDT were dissolved in 5 g distilled water separately. The two aqueous solutions were mixed while heated up to 50°C. Then the mixture solutions were poured into a 80mm × 60 mm PTFE mode. The water solvent was slowly evaporated at RT and followed with vacuum drying at 80°C for at least 24 h before transferring to the glove box. The membrane was then cut to round disks with a diameter of 9 mm and then immersed in the ionic liquid electrolytes (ILEs) for > 24 h at RT. The ILEs were prepared by adding the prescribed amounts of LiFSI to C_3mpyrFSI IL at RT in an Ar-filled glove box (< 0.01 ppm O_2 and < 0.01 ppm H_2O). The concentration of LiFSI in the ILEs employed in this work is 3.2 mol kg^{-1}.

Symmetric and full cells

The Li-metal symmetric coin cells were prepared with CR2032 cases with two 5 mm diameter Li-metal electrodes and 9 mm diameter IPEs (~ 50 μm) between them in an Ar-filled glove box. The Li|IPEs|Li symmetric coin cells were used for polarization, impedance spectroscopy and cycling measurements. The Li|IPEs|$LiFePO_4$ and Li|IPEs|Cu coin cells were also prepared for investigation of the electrochemical cycling performance, correspondingly. A Neware system were used for battery testing.

Cyclic voltammetry

A stainless steel working electrode and a Li-metal foil counter electrode were employed for cyclic voltammetry. The CV measurements were performed against $Li|Li^+$ redox potential. All scans were performed at RT with 10 mV s^{-1} scan rate using a Biologic VMP 3e controlled by EC-Lab (ver. 10.40) software.

Ionic conductivity

The ionic conductivity was measured via dielectric response over a 100 mHz – 1 MHz frequency range for the assemble coin cells with stainless steel as the electrodes. A temperature scan range − 50°C to 150°C was selected, and the temperature was controlled by an oven. The ionic conductivities of the IPEs were obtained by fitting the electrochemical impedance spectra to an equivalent circuit model using EC-Lab (ver. 13.40) software®.

Li Transference Number (t_{Li}^+): The transference number was determined by direct current (DC) polarization. An AC impedance test was firstly performed over a 100 mHz to 1 MHz range to obtain the interfacial resistance before and after the polarization. The Li symmetric cells were polarized at ambient temperature with a constant potential of 10 mV for 1 h to obtain a stable current.

Scanning electron microscopy was performed using a Zeiss Gemini SEM500 FESEM equipped with a Leica EM VCT500 microscope.

Declarations

Data availability

All data generated and analyzed in this study are included in this published article and its supplementary information files and are also available from the corresponding author on reasonable request. The codes for the machine learning workflow, Psi4 calculation and GCN predictions are available online at https://github.com/WangsGroupFDU/IL_machine_learning.

Acknowledgments

This work was supported primarily by the China National Natural Science Fund for Excellent Yong Scientists Fund Program and Pujiang Talents with award number 21PJD003.

Author contributions

YW conceived ideas, designed ML steps and composed and edited article drafts. KL and YYS assisted execution and analysis of the electrochemical experiments and edited article drafts. JW helped the organization and management of the ML code and edited article drafts.

References

1. Wang, Y. *et al.* Solid-state rigid-rod polymer composite electrolytes with nanocrystalline lithium ion pathways. Nature Materials **20**, 1255–1263, doi:10.1038/s41563-021-00995-4 (2021).
2. Lu, Y. Y., Korf, K., Kambe, Y., Tu, Z. Y. & Archer, L. A. Ionic-Liquid-Nanoparticle Hybrid Electrolytes: Applications in Lithium Metal Batteries. Angew Chem Int Edit **53**, 488–492, doi:10.1002/anie.201307137 (2014).
3. Watanabe, M. *et al.* Application of Ionic Liquids to Energy Storage and Conversion Materials and Devices. Chemical Reviews **117**, 7190–7239, doi:10.1021/acs.chemrev.6b00504 (2017).
4. Wu, F. *et al.* "Liquid-in-Solid" and "Solid-in-Liquid" Electrolytes with High Rate Capacity and Long Cycling Life for Lithium-Ion Batteries. Chem Mater **28**, 848–856, doi:10.1021/acs.chemmater.5b04278 (2016).
5. Armand, M., Endres, F., MacFarlane, D. R., Ohno, H. & Scrosati, B. Ionic-liquid materials for the electrochemical challenges of the future. Nature Materials **8**, 621–629, doi:Doi 10.1038/Nmat2448 (2009).
6. Wang, Y. *et al.* Highly Conductive and Thermally Stable Ion Gels with Tunable Anisotropy and Modulus. Adv Mater **28**, 2571-+, doi:10.1002/adma.201505183 (2016).
7. Kim, Y. S. Polymer Electrolytes with High Ionic Concentration for Fuel Cells and Electrolyzers. ACS Applied Polymer Materials **3**, 1250–1270, doi:10.1021/acsapm.0c01405 (2021).
8. Xiao, K. *et al.* Nanofluidic voidless electrode for electrochemical capacitance enhancement in gel electrolyte. Nat Commun **12**, 5515, doi:10.1038/s41467-021-25817-8 (2021).
9. Kim, O., Shin, T. J. & Park, M. J. Fast low-voltage electroactive actuators using nanostructured polymer electrolytes. Nat Commun **4**, 2208, doi:10.1038/ncomms3208 (2013).
10. Werber, J. R., Osuji, C. O. & Elimelech, M. Materials for next-generation desalination and water purification membranes. Nature Reviews Materials **1**, 16018, doi:10.1038/natrevmats.2016.18 (2016).
11. Wang, M. *et al.* Tough and stretchable ionogels by in situ phase separation. Nature Materials **21**, 359–365, doi:10.1038/s41563-022-01195-4 (2022).
12. Yang, C. *et al.* Copper-coordinated cellulose ion conductors for solid-state batteries. Nature **598**, 590–596, doi:10.1038/s41586-021-03885-6 (2021).
13. Bruce, P. G., Freunberger, S. A., Hardwick, L. J. & Tarascon, J. M. Li-O-2 and Li-S batteries with high energy storage (vol 11, pg 19, 2012). *Nature Materials* **11**, doi:10.1038/NMAT3237 (2012).
14. Maier, J. Nanoionics: ion transport and electrochemical storage in confined systems. Nature Materials **4**, 805–815, doi:10.1038/nmat1513 (2005).
15. Gao, X., Wu, F., Mariani, A. & Passerini, S. Concentrated Ionic-Liquid-Based Electrolytes for High-Voltage Lithium Batteries with Improved Performance at Room Temperature. **12**, 4185–4193, doi:https://doi.org/10.1002/cssc.201901739 (2019).

16. Lu, J. *et al.* A lithium–oxygen battery based on lithium superoxide. Nature **529**, 377–382, doi:10.1038/nature16484 (2016).
17. Famprikis, T., Canepa, P., Dawson, J. A., Islam, M. S. & Masquelier, C. Fundamentals of inorganic solid-state electrolytes for batteries. Nature Materials **18**, 1278–1291, doi:10.1038/s41563-019-0431-3 (2019).
18. Nørskov, J. K., Bligaard, T., Rossmeisl, J. & Christensen, C. H. Towards the computational design of solid catalysts. Nature Chemistry **1**, 37–46, doi:10.1038/nchem.121 (2009).
19. Curtarolo, S. *et al.* The high-throughput highway to computational materials design. Nat Mater **12**, 191–201, doi:10.1038/nmat3568 (2013).
20. Butler, K. T., Davies, D. W., Cartwright, H., Isayev, O. & Walsh, A. Machine learning for molecular and materials science. Nature **559**, 547–555, doi:10.1038/s41586-018-0337-2 (2018).
21. Ceder, G. Predicting Properties from Scratch. **280**, 1099–1100, doi:doi:10.1126/science.280.5366.1099 (1998).
22. Fung, V., Zhang, J., Juarez, E. & Sumpter, B. G. Benchmarking graph neural networks for materials chemistry. npj Computational Materials **7**, 84, doi:10.1038/s41524-021-00554-0 (2021).
23. Hu, Q. *et al.* Smart Materials Prediction: Applying Machine Learning to Lithium Solid-State Electrolyte. Materials (Basel, Switzerland) **15**, doi:10.3390/ma15031157 (2022).
24. Carrera, G. & Aires-de-Sousa, J. Estimation of melting points of pyridinium bromide ionic liquids with decision trees and neural networks. Green Chemistry **7**, 20–27, doi:10.1039/B408967G (2005).
25. Venkatraman, V. *et al.* Rapid, comprehensive screening of ionic liquids towards sustainable applications. Sustainable Energy & Fuels **3**, 2798–2808, doi:10.1039/C9SE00472F (2019).
26. Dhakal, P. & Shah, J. K. A generalized machine learning model for predicting ionic conductivity of ionic liquids. Molecular Systems Design & Engineering, doi:10.1039/D2ME00046F (2022).
27. Koutsoukos, S., Philippi, F., Malaret, F. & Welton, T. A review on machine learning algorithms for the ionic liquid chemical space. Chemical Science **12**, 6820–6843, doi:10.1039/D1SC01000J (2021).
28. Nilsson-Hallén, J., Ahlström, B., Marczewski, M. & Johansson, P. Ionic Liquids: A Simple Model to Predict Ion Conductivity Based on DFT Derived Physical Parameters. **7**, doi:10.3389/fchem.2019.00126 (2019).
29. Liu, T., Johnson, K. R., Jansone-Popova, S. & Jiang, D.-e. Advancing Rare-Earth Separation by Machine Learning. JACS Au **2**, 1428–1434, doi:10.1021/jacsau.2c00122 (2022).
30. Zhang, Y. *et al.* Unsupervised discovery of solid-state lithium ion conductors. Nat Commun **10**, 5260, doi:10.1038/s41467-019-13214-1 (2019).
31. Rakov, D. A. *et al.* Engineering high-energy-density sodium battery anodes for improved cycling with superconcentrated ionic-liquid electrolytes. Nature Materials **19**, 1096–1101, doi:10.1038/s41563-020-0673-0 (2020).
32. Basile, A., Bhatt, A. I. & O'Mullane, A. P. Stabilizing lithium metal using ionic liquids for long-lived batteries. Nat Commun **7**, ncomms11794, doi:10.1038/ncomms11794 (2016).

33. Wołos, A. *et al.* Computer-designed repurposing of chemical wastes into drugs. Nature **604**, 668–676, doi:10.1038/s41586-022-04503-9 (2022).
34. Turney, J. M. *et al.* Psi4: an open-source ab initio electronic structure program. **2**, 556–565, doi:https://doi.org/10.1002/wcms.93 (2012).
35. Ong, S. P., Andreussi, O., Wu, Y., Marzari, N. & Ceder, G. Electrochemical Windows of Room-Temperature Ionic Liquids from Molecular Dynamics and Density Functional Theory Calculations. Chem Mater **23**, 2979–2986, doi:10.1021/cm200679y (2011).
36. Miller, C. C. The Stokes-Einstein Law for Diffusion in Solution. *Proceedings of the Royal Society of London. Series A, Containing Papers of a Mathematical and Physical Character* **106**, 724–749 (1924).
37. Yu, D., Zanelotti, C. J., Fox, R. J., Dingemans, T. J. & Madsen, L. A. Solvent-Cast Solid Electrolyte Membranes Based on a Charged Rigid-Rod Polymer and Ionic Liquids. ACS Applied Energy Materials **4**, 6599–6605, doi:10.1021/acsaem.0c03133 (2021).
38. Suo, L. *et al.* "Water-in-salt" electrolyte enables high-voltage aqueous lithium-ion chemistries. Science **350**, 938–943, doi:10.1126/science.aab1595 (2015).
39. Evans, J., Vincent, C. A. & Bruce, P. G. Electrochemical measurement of transference numbers in polymer electrolytes. Polymer **28**, 2324–2328, doi:https://doi.org/10.1016/0032-3861(87)90394-6 (1987).
40. Yoon, H., Howlett, P. C., Best, A. S., Forsyth, M. & MacFarlane, D. R. Fast Charge/Discharge of Li Metal Batteries Using an Ionic Liquid Electrolyte. J Electrochem Soc **160**, A1629-A1637, doi:10.1149/2.022310jes (2013).
41. Fu, C. *et al.* A Polymerized-Ionic-Liquid-Based Polymer Electrolyte with High Oxidative Stability for 4 and 5 V Class Solid-State Lithium Metal Batteries. **12**, 2200412, doi:https://doi.org/10.1002/aenm.202200412 (2022).
42. Xiao, J. *et al.* Understanding and applying coulombic efficiency in lithium metal batteries. Nature Energy **5**, 561–568, doi:10.1038/s41560-020-0648-z (2020).
43. Zhang, X.-Q. *et al.* Columnar Lithium Metal Anodes. Angewandte Chemie International Edition **56**, 14207–14211, doi:https://doi.org/10.1002/anie.201707093 (2017).
44. Ko, S. *et al.* Electrode potential influences the reversibility of lithium-metal anodes. Nature Energy, doi:10.1038/s41560-022-01144-0 (2022).
45. Gao, J. W. *et al.* Water and sodium transport and liquid crystalline alignment in a sulfonated aramid membrane. J Membrane Sci **489**, 194–203, doi:10.1016/j.memsci.2015.03.090 (2015).
46. Wang, Y., Gao, J., Dingemans, T. J. & Madsen, L. A. Molecular Alignment and Ion Transport in Rigid Rod Polyelectrolyte Solutions. Macromolecules **47**, 2984–2992, doi:10.1021/ma500364t (2014).

Figures

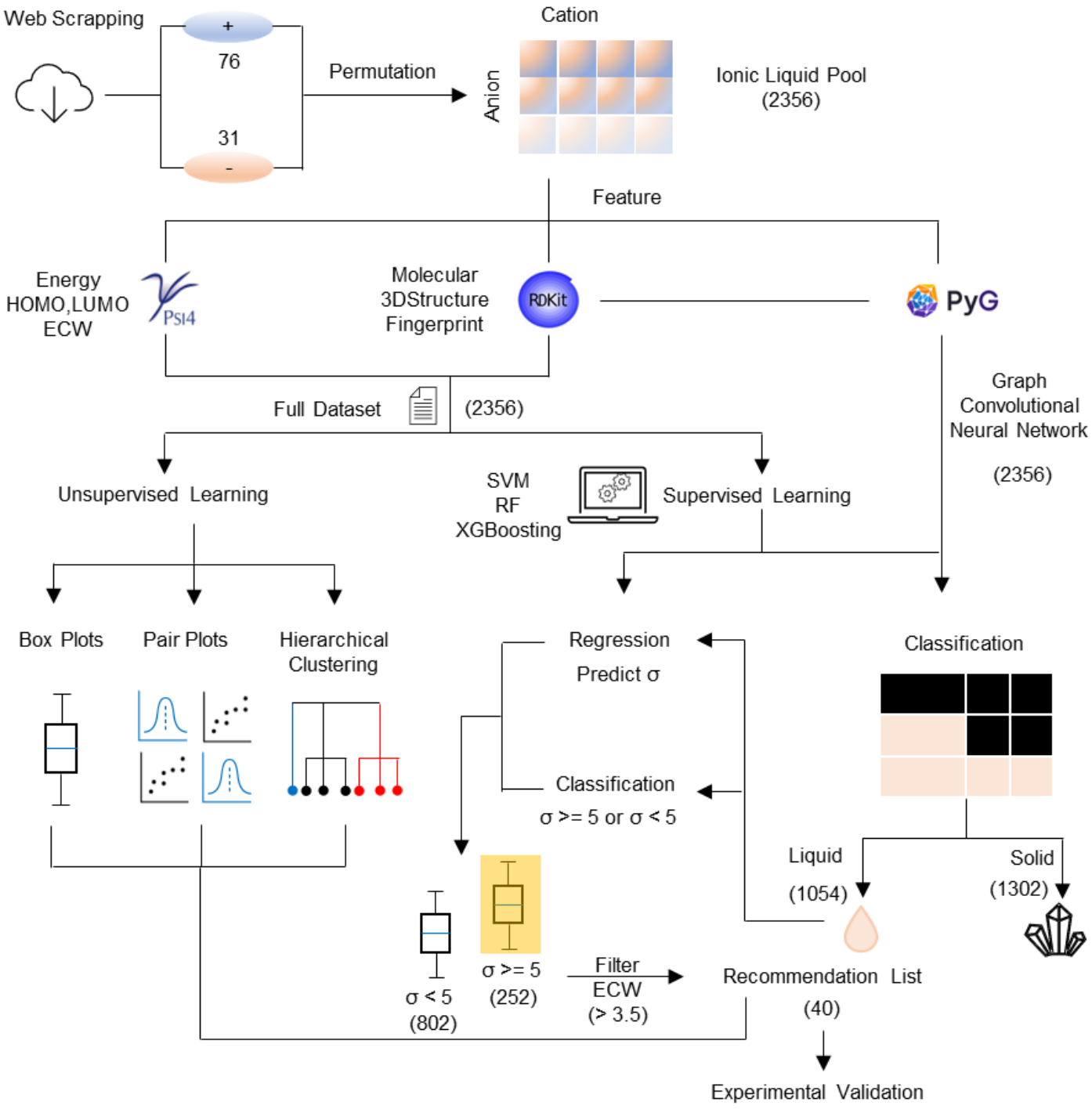


Figure 1

Machine learning workflow for the discovery of ILs with high conductivity (σ) and wide electrochemical window (ECW). The permutation of 76 cations and 31 anions forms an IL pool with 2356 unique ILs. Three open-source platforms, including RDKit, Psi4 and PyG are employed to generate the molecular descriptors of the raw dataset. This workflow mainly includes unsupervised learning and supervised learning. The unsupervised learning contains boxplots, pair plots and hierarchical clustering, which are essential analytical methods to investigate the structure and correlations of variables in the dataset. The supervised learning takes advantage of both regression and classification based on SVM, RF, XGBoosting

and GCN. The IL pool will be initially classified as solid or liquid clusters. Then the ILs with liquid phase at RT will be further classified based on the σ value ≥ 5 mS cm^{-1} or not. Meanwhile, we also utilized regression to predict the absolute σ values of the ILs for reference. At last, the ECW values > 3.5 V is the final screening criterion before we finalize the recommendation list.

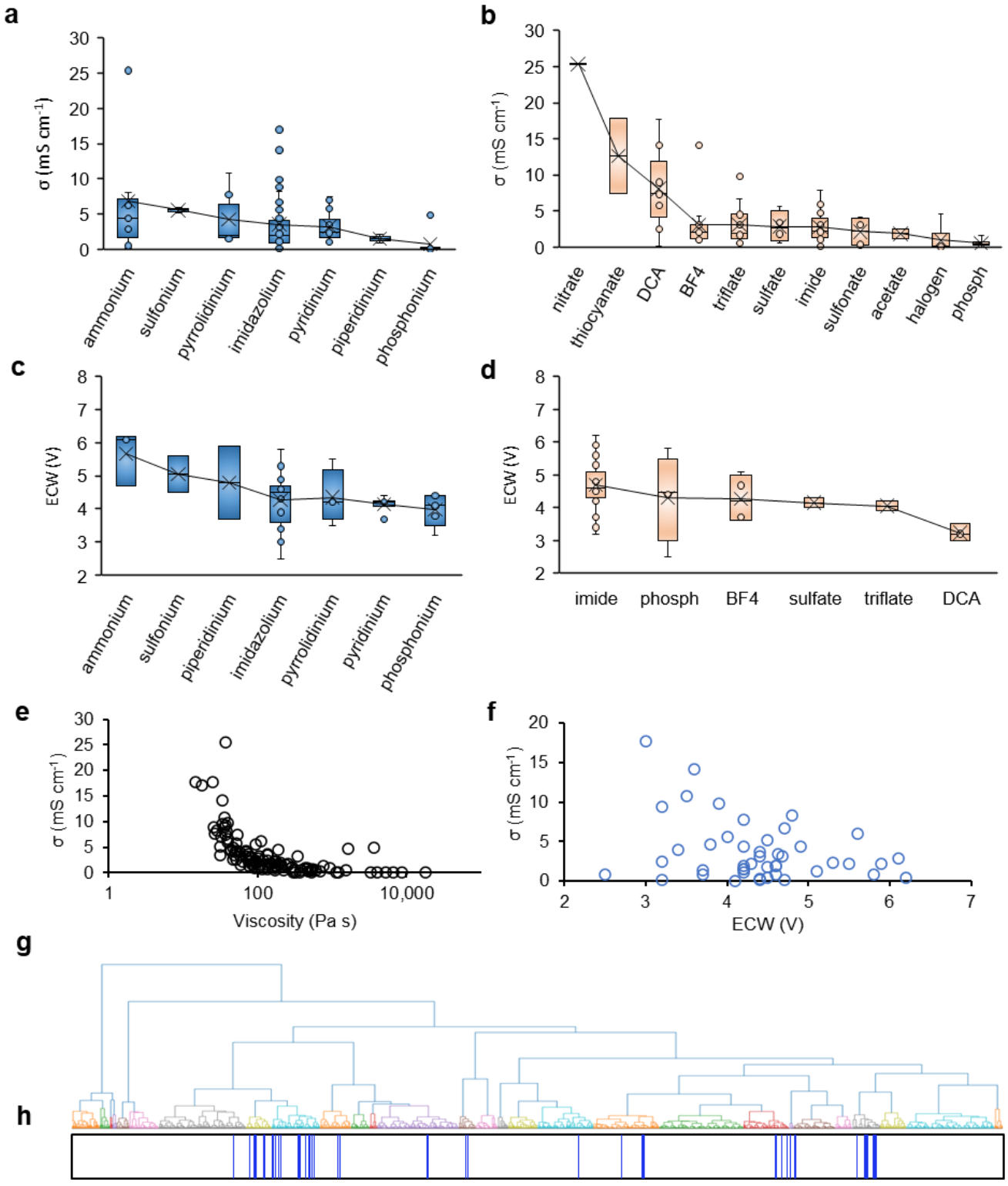


Figure 2

Unsupervised learning of the dataset. (a, b) The boxplots of the ILs with known conductivity (σ) classified by the cation and anion types, corresponding. (c, d) The boxplots of the ILs with known ECWs classified by the cation and anion types, correspondingly. (e) The relationship between the σ and the viscosity of the ILs. (f) The relationship between the σ and the ECW of the ILs. (g) Hierachical clustering dendrogram for the ILs based on calculated ECWs and top 10 features of conductivity classification task. (h) The blue lines show the screened ILs based on the supervised learning section introduced in the following section. The blue lines are highly consistent with the clustering results achieved by the unsupervised learning.

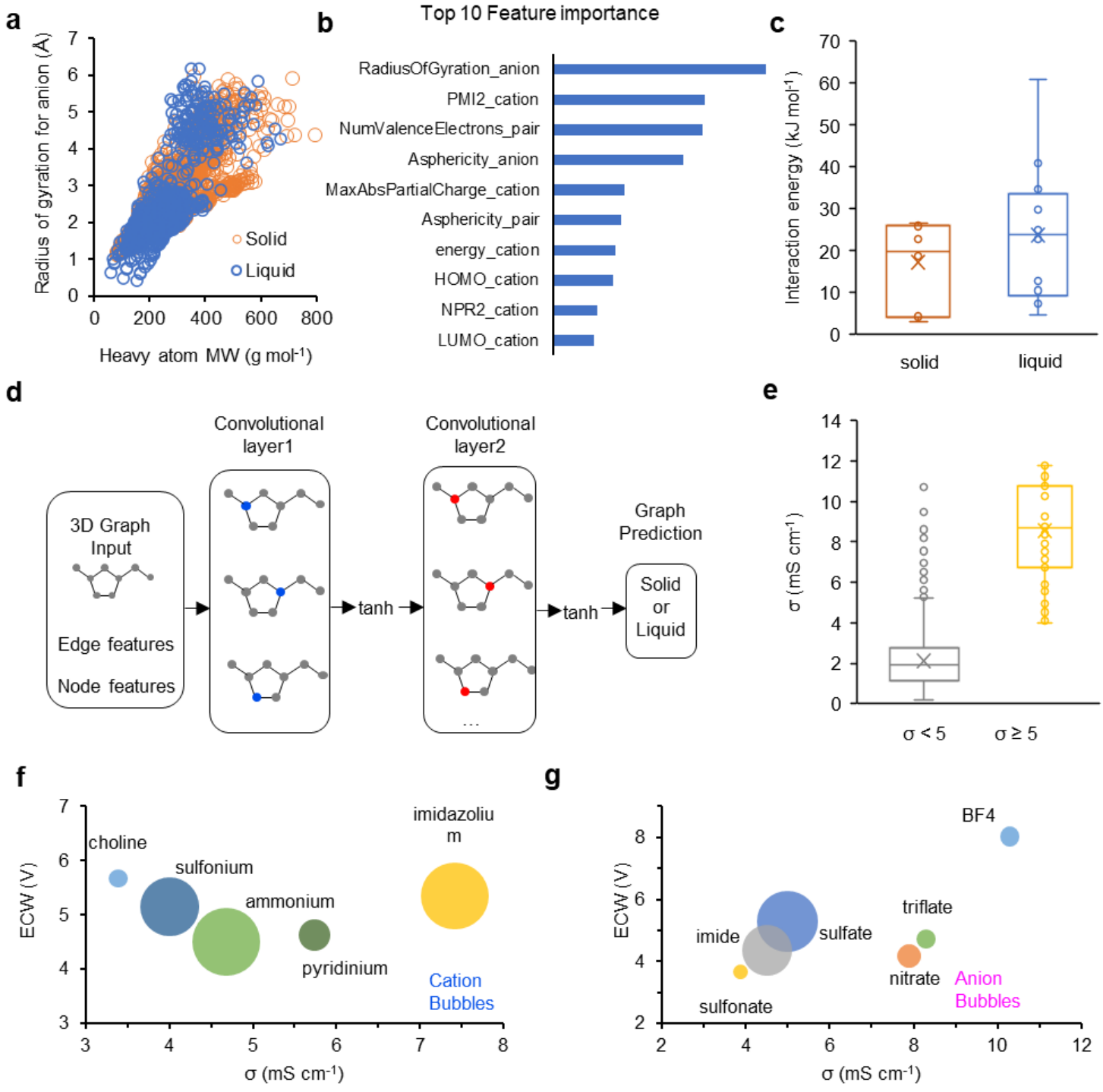


Figure 3

Supervised learning of the dataset. (a) The relationship between the radii of gyration and the heavy atom molecular weights for the ion pairs with solid or liquid labels based on the classification. (b) The top 10 important features of the XGBoosting model for the classification of solid or liquid. (c) The interaction energies between cations and anions for ILs randomly selected from the predicted solid and liquid clusters. (d) The diagram for the GCN workflow with two hidden layers followed with two tanh activation layers. (e) The boxplots of predicted σ for the two categories with σ ≥ 5 mS cm^{-1} or not. (f,g) The bubble plots show the relationship between ECW and σ of the final recommended ILs grouped by the cation and anion types, separately. The bubble size refers to the count of ILs in each category.

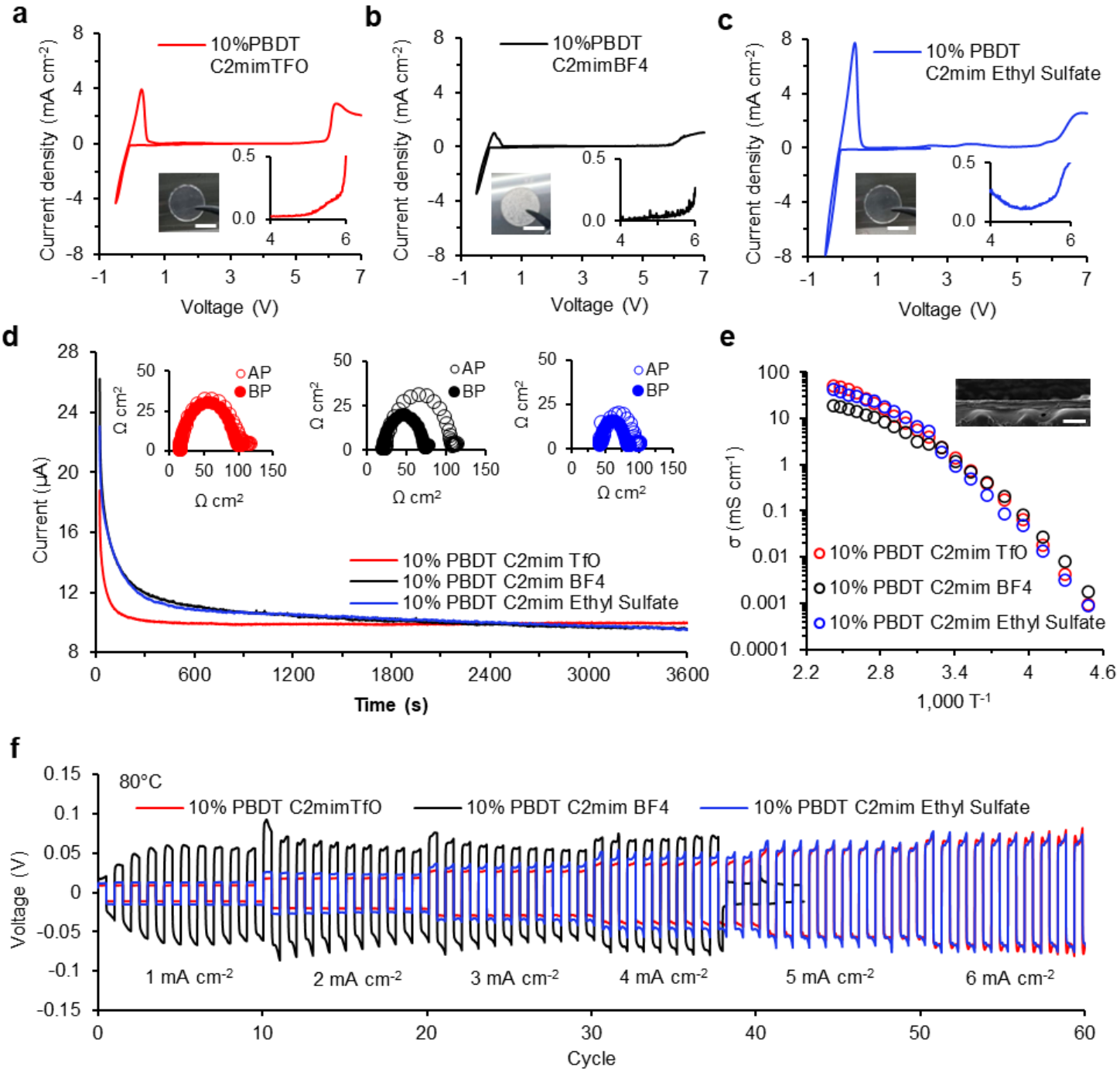


Figure 4

Electrochemical window, Li^+ transference number, interfacial charge-transfer resistance, ionic conductivity and Li symmetric cell cycling performance in IPEs. (a-c) Cyclic voltammetry curves for Li plating and stripping in IPEs with C_2mimTFO, C_2mimBF_4, C_2mim Ethyl Sulfate at sweep rate of 10 mV s^{-1}. Inset plots show the enlarged view of the cycles in the high voltage range. The scale bar in the photo is 5 mm. (d) Steady-state current in symmetric Li|10%-IPEs|Li cell under 10 mV polarization. The insets are corresponding impedance spectra scanned before and after the polarization experiments. The frequency range used is 1Hz – 1MHz. (e) Arrhenius plots for ionic conductivity values of the three IPEs. The thickness of the IPEs (~ 50μm) is characterized by SEM as shown in the inset. The scale bar is 100 μm. (f) Cell voltage versus time for a symmetric Li||Li cell with the three IPEs at current densities (*J*) from 1 to 6 mA·cm^{-2} with changes in *J* every 10 cycles at 80°C (each cycle lasts 1 h).

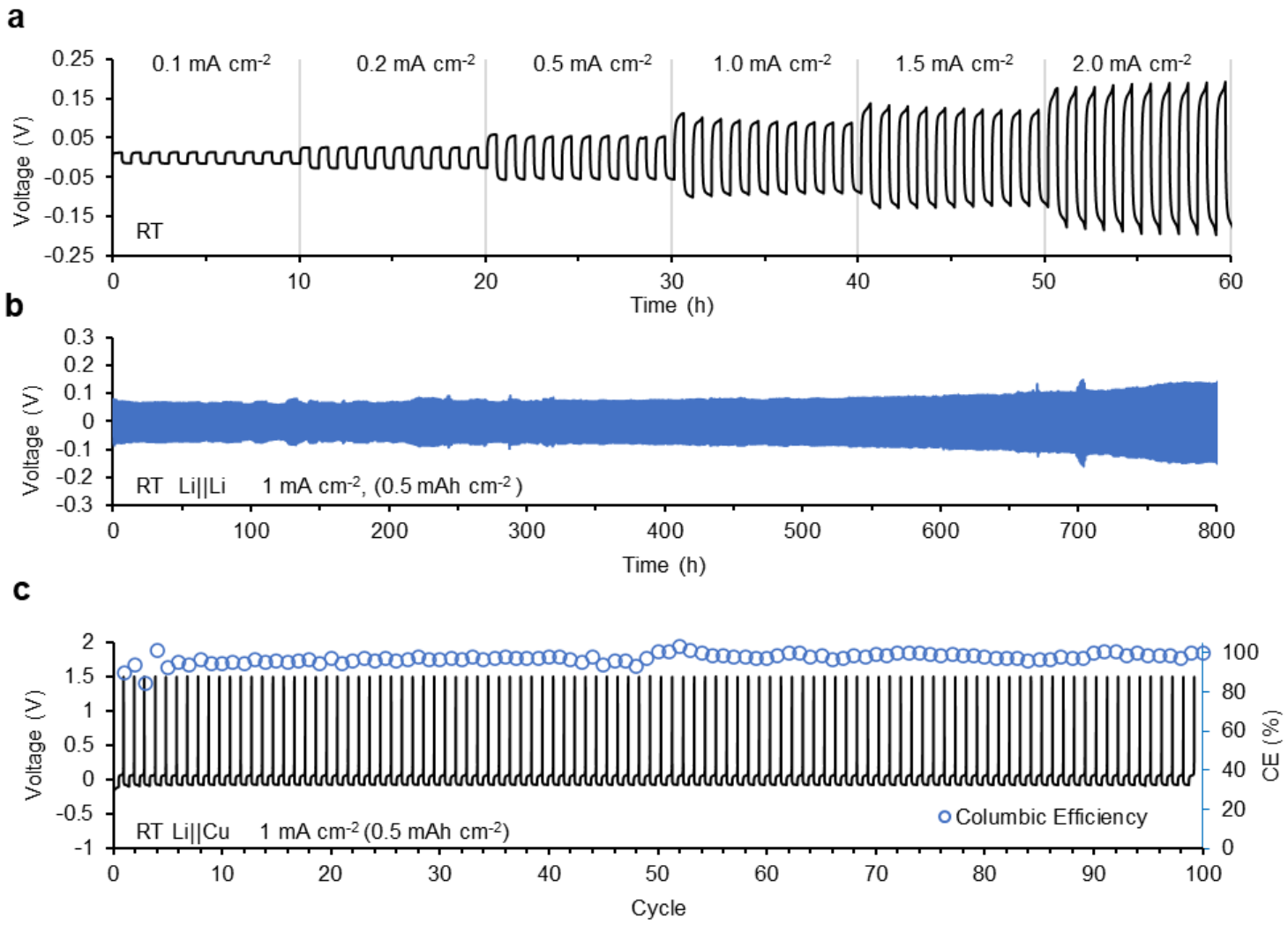


Figure 5

(a) Voltage-time profile for Li|IPEs|Li cell with increasing *J* from 0.1 to 2.0 mA cm^{-2} at RT. (a) Long-term voltage-time profile for Li|IPEs|Li cell with 1 mA cm^{-2} at RT. (c)Voltage-cycle profile for Li|IPEs|Cu cell at RT. The secondary axis shows the corresponding CE values, the average value of which is > 98%. (c)The long-term cycling performance of Li|IPEs|$LiFePO_4$ at 0.5C at RT. The black circles show the specific

capacity as a function of increasing cycle number. The blue circles display the CE for each cycle correspondingly.

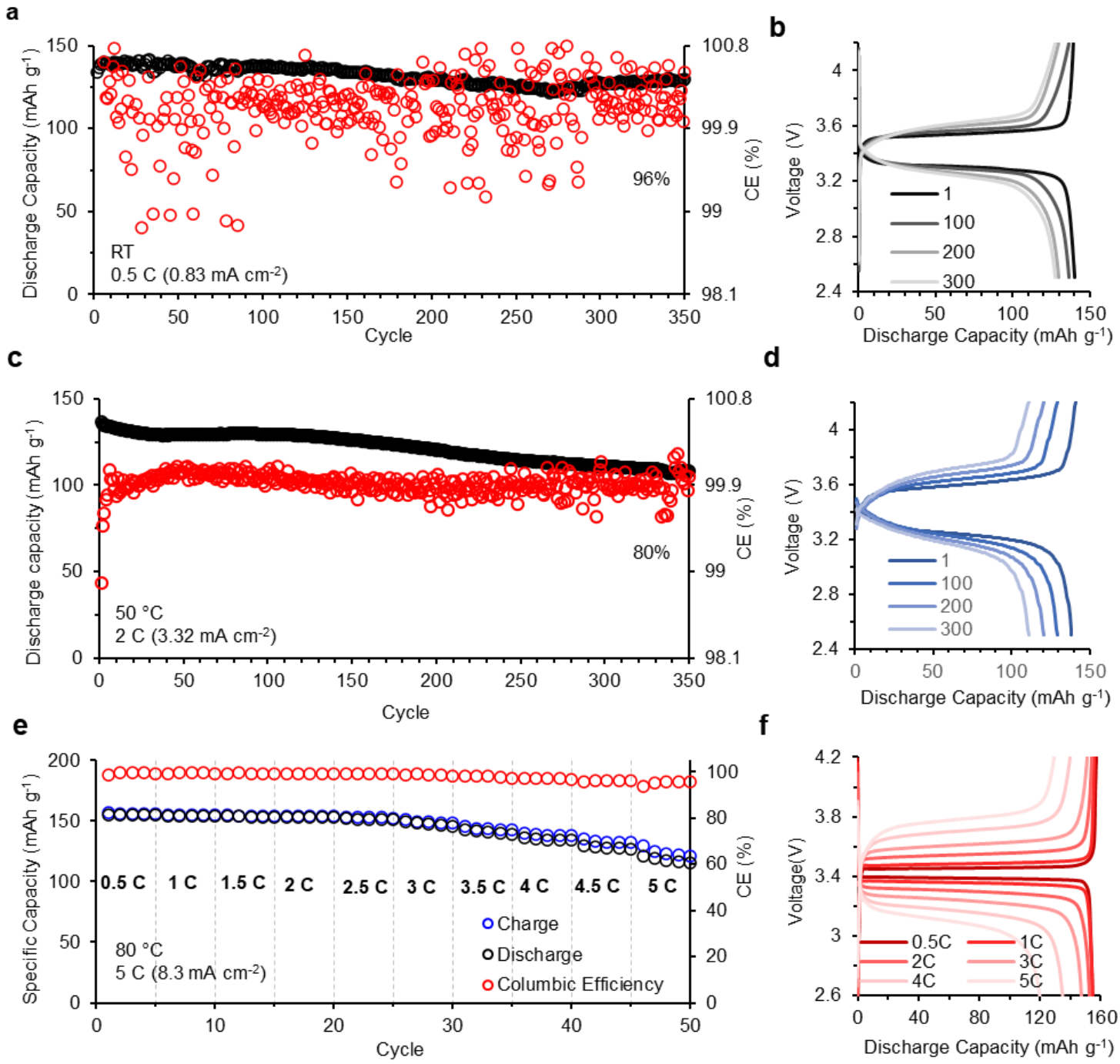


Figure 6

(a) The long-term cycling performance of Li|IPEs|$LiFePO_4$ cell at 0.5C (0.83 mA cm^{-2}) at RT. The black circles show the specific discharge capacity as a function of the increasing cycle number. The red circles display the CE for each cycle correspondingly. (b) The voltage-capacity profiles for the main cycles in (a). (c) The long-term cycling performance of Li|IPEs|$LiFePO_4$ at 2 C (3.32 mA cm^{-2}) at 50 °C. (d) The voltage-

capacity profiles for the main cycles in (c). (e) The Li|IPEs|$LiFePO_4$ cell cycling profile at elevated rates from 0.5C to 5C (8.3 mA cm^{-2}) at 80 °C, which verifies the safety usage of this electrolyte at high temperature. (f) The voltage-capacity curves for the main cycles shown in (e).

Supplementary Files

This is a list of supplementary files associated with this preprint. Click to download.

- WangMLPolymerElectrolytesupporting20221031.docx